Received: 18 November 2022 | Revised: 26 January 2023 | Accepted: 26 January 2023

DOI: 10.1111/jmi.13173

Journal of Microscopy RMS

ORIGINAL ARTICLE

The structure of the eggshell and eggshell membranes of *Crocodylus niloticus*

A V Lensink[1] | **G E Swan**[2] | **J G Myburg**[2]

[1]Electron Microscope Unit, Faculty of Veterinary Sciences, Department of Anatomy and Physiology, University of Pretoria, Pretoria, South Africa

[2]Exotic Leather Research Centre, Faculty of Veterinary Science, Department of Paraclinical Sciences, University of Pretoria, Pretoria, South Africa

Correspondence
A V Lensink, Electron Microscope Unit, Faculty of Veterinary Sciences, Department of Anatomy and Physiology, University of Pretoria, Pretoria, South Africa.
Email: antoinette.lensink@up.ac.za

Abstract

The macro- and microstructure, elemental composition, and crystallographic characteristics of the eggshell and eggshell membranes of the *Crocodylus niloticus* egg was investigated using optical and electron microscopy, energy-dispersive X-ray spectroscopy (EDS), electron backscatter diffraction (EBSD) and computerised tomography. The translucent ellipsoid egg is composed of two basic layers, the outer calcified layer referred to as the shell and an inner organic fibre layer, referred to as the shell membrane. The outer inorganic calcite shell is further divided into an external, palisade and mammillary layers with pore channels traversing the shell. The external layer is a thin layer of amorphous calcium and phosphorus, the underlying palisade layer consist of irregular wedge-shaped crystals composed calcite with traces of magnesium, sodium, sulphur and phosphorus. The crystals are mostly elongated, orientated perpendicular to the shell surface ending in cone-shaped knobs, which forms the inner mammillary layer. The elemental composition of the mammillae is like that of the palisade layer, but the crystal structure is much smaller and orientated randomly. The highest number of mammillae and shell pores are found at the equator of the egg, becoming fewer towards the egg poles. The shell thickness follows the same pattern, with the thickest area located at the equator. The eggshell membrane located right beneath and embedded in the mammillary layer of the shell; it is made up of unorganised fibre sheets roughly orientated at right angles to one another. Individual fibres consist of numerous smaller fibrils forming open channels that run longitudinally through the fibre.

KEYWORDS

computed tomography, *Crocodylus niloticus*, egg, electron backscatter diffraction, electron microscopy, energy-dispersive X-ray spectroscopy, light microscopy

1 | INTRODUCTION

Amniotes are a biological group consisting of reptiles, birds and a few mammals, the evolution of their reproduction mechanism; the amniotic egg is an important transition in the adaptation from exclusively aquatic to terrestrial reproduction capabilities. Amniotes produce fertilised eggs with extra-embryonic membranes suitable

for embryonic development outside their reproductive tracts or body cavities and independent from water. The egg serves four basic functions: (1) conduction of respiratory gasses, heat, light and sound; (2) modulation of water uptake and loss; (3) protection from the external physical and microbial environment and (4) provision of calcium and other minerals for the developing embryo.[1,2,3,4]

The structure of the protective extra-embryonic layers produced by widely heterogeneous amniotic species vary significantly, but is divided into three basic categories based on the physical properties and composition of the eggshell:[5,6,7,8,9] Parchment-shelled eggs as seen in most squamates consists of an organic fibrous shell membrane. Flexible eggshells consisting of an organic fibrous shell membrane and poorly organised calcareous matter as found in all turtles and some chelonians. Lastly, calcareous eggshells found in avian, crocodilian, gekkotans, some chelonians and nonextant dinosaurian eggs, composed of a fibrous shell membrane and a thick calcareous layer. Extant calcareous eggshells share similar histostructural organisations and can be classed into four basic types, testudoid, geckonoid, crocodiloid and ornithoid.[10,11,12,13] Fossil egg histostructure differs somewhat and is classed into a further three types namely dinosauroid spherulitic, dinosauriod prismatic and an ornithoid type which is linked to the extant organisation type. Within these basic types, 14 different morphotypes (four from extant species) has been described according to the following structural levels:[7]

- The ultrastructure – the organisation of the calcareous material as a sequence of horizontal zones (e.g. zone of crystalline or squamatic elements) combined with the layers of organic fibres (membrane).
- The microstructure – the histomorphology of the calcareous material (e.g. organic core, eisospherite, mammillae, prisms or wedges) and the pore system arrangement.
- The macrostructure – the general parameters of the egg, such as shape and shell thickness.

Comprehensive morphological and structural description and understanding of species-specific eggshells and their associated membrane is of not only parataxonomic and evolutionary, but also of biological and functional importance as the structural properties and physical characteristics of the eggshell and membrane determine hatching success of the amniote egg.[14,15] For example, macroparameters such as surface area, volume and mass partially regulate gas and water exchange rates,[16] knowledge of which aids in assessing incubation requirements.[17] Knowledge of crystallographic texture and features such as crystal orientation, size, shape, initiation, and mode of growth, which ultimately govern shell strength are important in understanding the biomineralisation process and the physiological needs of this process.[18,19,20] The porosity also influence the mechanical strength of the egg[21] and is determined by the density and distribution of the structural elements, the mammillae, on the interior surface of the eggshell.[22,23,24] The organic membranes fibrillary design in turn contributes to properties of the amniotic eggs ability to incubate and protect the developing embryo. In certain species the undulating nature of the membrane allow for water uptake in humid conditions.[25,9,26] Interfibrillar cavities contribute to the elasticity or rigidity of fibrils aiding in structural integrity[27] and variation of ratios of fibrils-to-intrafibrillary space could also be indicative of adhesive and cohesive properties of the eggshell.[26] Hollow fibres support thermoregulation and insulation[27] and has been suggested to reduce the amount of protein invested in the shell membrane which support the efficacy of egg production.[28] The disposition and configuration of the eggshell membrane also allows for the prediction of where the inorganic seeding will take place and in which direction crystal growth will occur.[29]

The Nile crocodile (*Crocodylus niloticus*) is one of the largest and well-known crocodilians in the world. It is native to Africa and is found widespread over the continent (Angola, Botswana, Burundi, Cameroon, Congo, Democratic Republic of Congo, Egypt, Eritrea, Ethiopia, Equatorial Guinea, Gabon, Kenya, Madagascar, Malawi, Mozambique, Namibia, Rwanda, Somalia, South Africa, South Sudan, Sudan, Swaziland, Tanzania, Uganda, Zambia and Zimbabwe) and in the Northwest region of Madagascar.[30,31,32,33] *C. niloticus* is an important part of the ecosystems they form a part of and is a 'keystone specie' that aids in the maintenance of the structure and function of their respective environments and ecological communities.[34,35] This species is also widely farmed in Africa for its skin and meat, making it economically important to several third-world countries.

Knowledge of the microstructural and ultrastructural features of the eggshell and eggshell membrane of this species is limited and mostly based on extrapolations from studies of conducted on similar species such as the American alligator. Therefore, in the current study, we investigated the macro-, micro-, ultrastructure, elemental composition and crystallographic characteristics of the eggs of *C. niloticus* using optic and electron microscopy, energy-dispersive X-ray spectroscopy (EDS), electron backscatter diffraction (EBSD) and computerised tomography.

This data will enhance current knowledge into the reproductive biology, embryology and reproductive pathology of the species in question and may be of value to farming ventures, aiding in optimisation of husbandry practices, egg handling and incubator conditions, ultimately contributing to the overall value chain and economic success of farming practices.

2 | MATERIAL AND METHODS

Sixty-two crocodile eggs from 34 different nesting sites on three South African commercial crocodile farms were collected shortly after oviposition (Animal Ethics Committee – Certificate number V118-16). Egg collection was carried out in accordance with the South African National Standard for crocodiles in captivity, SANS 631:2009.[36]

2.1 | Macrostructure

Fifty eggs from 22 different nesting sites were used for macrostructural parameter determination. The egg weight, g (M), length, mm (L), width, mm (W) and measured volume cm^3 (MV) were determined using a calibrated laboratory scale, digital micrometre calliper and the water replacement method. Assuming an ellipsoidal-shaped egg, further calculations were made from the measurements. Calculated volume cm^3 (V) were determined using the following equation.[37]

$$V = Kv^1 LW^2,$$

where $Kv1$ equals a variable coefficient, used to compensate for the deviation of the reptile egg shape from a true ellipsoid. The variable coefficient is calculated from the ellipsoid constant ($Kve = 0.5236$) using the following equation (El = elongation factor L/W).[37]

$$Kv^1 = Kve + \left(Kve \times \frac{2El}{100}\right).$$

Surface area cm^2 (S) of the egg was calculated using the following equations.[17]

$$S = \pi W \left(W + \frac{\text{Larccos}\left(\frac{W}{L}\right)}{\sqrt{L^2 - W^2}}\right)/2.$$

To confirm the assumed shape, length-to-width ratios were also calculated (characterised as spherical, elliptical, and oblong if they have ratios 1.00 to 1.10, 1.10 to 1.99 and 2.00 to >2.00, respectively).

2.2 | Microstructure

Twelve eggs from 12 different nesting sites were segmented into five zones each based on their region, named A, B, C, D and E (pole A, intermediate area B, equator C, intermediate area D and pole E). Each area was further apportioned, and the eggshell fragments allocated to each analysis method.

2.2.1 | Stereo light microscopy

Eggshell samples (approximately 2 × 2 cm) from 6 eggs (total of 30 samples) were washed with phosphate buffer to remove any debris, and the membrane removed by manually striping the membrane from the shell matrix and submerging the shell in sodium hydroxide for 15 min at 100°C. For mammillae, imaging and counting the fragments were imaged as is, and for pore channel analyses an aqueous solution of toluidine blue was applied to the interior surface of the eggshell. Imaging was done with an Olympus SZX16 stereoscopic microscope (Olympus Corporation, Tokyo, Japan).

2.2.2 | Transmitted light microscopy and transmission electron microscopy (TEM)

Eggshell samples (approximately 2 × 4 mm) from 6 eggs (total of 30 samples per imaging method) were washed with phosphate buffer to remove any debris such as nesting or incubation material and fixed with a phosphate buffered 2.5% glutaraldehyde, 2.5% formaldehyde solution for 2 h. To protect the shell-membrane association during further processing, the samples was encased in 2% agar followed by decalcification with 10% buffered formic acid for 24 h at 4°C. Samples were washed, post fixated with 1% osmium tetroxide (2 h), dehydrated in a graded series of ethanol and infiltrated with a 3:1 ratio of 100% ethanol and epoxy (Agar 100) resin (2 h). The mixture was replaced with a 3:2 ratio of 100% ethanol and resin (4 h), after which the mixture was again replaced with pure resin and left overnight at 4°C. Fresh resin was used to polymerise the samples in TEM block moulds (36 h at 60°C). For light microscopy thin (0.3 µm) sections were cut (Leica EM UC7 ultramicrotome, Leica Microsystems GmbH, Wetzlar, Germany), stained with toluidine blue, mounted onto a microscope slide with entellan and viewed and imaged with an Olympus BX63 transmitted light microscope (Olympus Corporation, Tokyo, Japan). For TEM, ultrathin (0.1 µm) sections were cut, stained with uranyl acetate for 6 min followed by 3 min of staining with lead citrate and viewed with a Philips CM10 TEM (Philips Electron Optical Division, Eindhoven, Netherlands) at 80 kV. iTEM software (Olympus Soft Imaging Solutions, Münster, Germany) was used to measure the individual fibre sizes in the eggshell membrane from each sample.

2.2.3 | Polarised light microscopy, EDS and EBSD sample preparation

Samples were prepared similarly to transmitted light and transmission electron microscopy samples apart from the

resin used. After dehydration, the samples were infiltrated with a 4:1 ratio of 100% ethanol and Durcupan resin for 2 h, followed by a 2:1 mixture overnight at 4°C, a 1:1 mixture for 8 h, a 1:2 mixture overnight at 4°C. The mixture was removed and replaced with pure resin and left for 24 h at 4°C, again replaced with freshly prepared resin, and allowed to polymerise for 48 h at 60°C in large moulds containing 15 parallelly arranged shell sections. For polarised light microscopy, thin sections were made by reducing the block thickness to roughly 0.5 mm with a circular blade and polishing the sample using a sequence of successively finer (6 to 0.25 μm) particle size diamond polishing pastes and a lap wheel covered with a low relief polishing cloth. The sample was then imaged using a Zeiss AXIO Imager M2 polarised light microscope (Zeiss, Oberkochen, Germany). EDS and EBSD samples were polished in a similar approach followed by 20 min of polishing with colloidal silica (0.06 μm) and carbon coating. EBSD was performed using the Nordlys Detector (Oxford Instruments, High Wycombe, UK) (accelerating voltage 30 Kv, working distance 25.0 mm, and a 70° tilting angle of the specimen) and EDS using an X-Max^N detector (Oxford instruments, High Wycombe, UK) (10 kV accelerating voltage, 8.0 mm working distance) both attached to a Zeiss Gemini Ultra Plus SEM. For the EBSD analysis, the Kikuchi lines were automatically indexed using AZtecSynergy software (Oxford Instruments, High Wycombe, UK) applying a grid spacing of 0.8 μm. EBSD data are presented in diffraction intensity and inverse pole figure (IFP) maps, where the red areas represent crystals with a *c*-axis perpendicular to the eggshell surface and blue to green colouring crystals with a horizontally aligned *c*-axis.

2.2.4 | Scanning electron microscopy (SEM)

Eggshell samples (approximately 2 × 2 cm) from 6 eggs (total of 30 samples for each preparation method used and orientation/feature imaged) were washed with phosphate buffer to remove debris such as nesting or incubation material and placed into a phosphate buffered 2.5% glutaraldehyde, 2.5% formaldehyde solution for 2 h, washed with phosphate buffer, dehydrated in a graded series of ethanol, and dried using HDMS. Dried samples were mounted in several orientations corresponding to the area of interest to be imaged (external/internal shell surface/membrane/cross-sectional) using aluminium paint on standard SEM stubs. To image the mammillary knobs, the membrane was manually removed with forceps or submerged in sodium hydroxide for 15 min at 100°C to remove any residual organic components. To image freshly fracture surfaces of the shell, a collection of samples was plunged into liquid nitrogen immediately after the initial buffer wash, fractured and freeze dried. To examine the eggshell membrane in transverse without any mechanical damage, dehydrated samples were embedded in paraffin wax and carefully trimmed using a microtome blade. The wax was then dissolved in xylene and the sample dried using HDMS as above. To image the pore channels the eggshell membrane was manually removed from the shell using forceps and any residual organic components dissolved by submerging the sample in sodium hydroxide for 15 min at 100°C. The shells were rinsed with deionised water, and air-dried. When drying was complete, the shell was placed in an aluminium weigh boat and several drops of a low viscosity polymer epoxy resin (Agar 100) applied to the mammillary surface of the eggshell and allowed to polymerise at 60°C for 36 h. The shell was decalcified using 3N hydrochloric acid (30–60 min) and the epoxy cast rinsed with ddH_20 and allowed to dry at room temperature. The samples and casts were mounted on standard SEM aluminium stubs using silver paint, carbon coated and imaged using a Zeiss Crossbeam 540 High Resolution (Zeiss, Oberkochen, Germany) scanning electron microscope (SEM) at 1 kV with an average working distance of 4 mm.

2.2.5 | Micro- and nano-CT

For micro-CT, samples (approximately 2×2 cm) from 3 eggs (total of 15 samples) were washed, mounted in a radiolucent foam and placed in phosphate buffered 2.5% glutaraldehyde, 2.5% formaldehyde. The sample secured in foam was placed onto the sample stage and scanned at an energy beam of 100 kV and 100 μA with a detector distance of 82.5 mm using the Nikon XTH 225 ST microfocus X-ray tomography (MICRO-CT) machine (Nikon Metrology, Leuven, Belgium), housed at the Microfocus X-ray Radiography and Tomography facility (MIXRAD) of the South African Nuclear Energy Corporation (Necsa) at Pelindaba (Hoffman and de Beer, 2012). The samples were scanned with a 0.125-mm-thick aluminium filter, a scan rotation of 360°, average scanning time of 25 min and a resolution of 16 μm. A total of 1000 projection images were collected with a 2000 ms exposure and frame average of 3. For nano-CT analyses, shell fragments (approximately 2×2 mm) from 1 egg (total of 5 samples) without the membrane were scanned with a General Electric Phoenix Nanotom S System (R-CON NDT, Menomonie, Wisconsin, USA) housed at the Stellenbosch CT Facility. The sample was scanned at a voxel resolution of 0.5 μm and a beam energy of 60 kV and 430 μA with a molybdenum anode. A total of 2000 projection images were collected with a 2000 ms exposure.

VG StudioMAX v2.2 package (Volume Graphics, GmbH, Heidelberg, Germany) was used for al image processing and analysis. 2D projection images were reconstructed into a 3D volume using Nikon CT-Pro (XTELCTPro 3D version XT22 – CopyrightV R Nikon Metrology 2004–2011) based on cone-beam filtered back projection algorithms. Volumetric data, which consisted of individual voxels (3D pixels) mapped to a 16-bit grey level scale, was loaded into VG StudioMAX as unsigned 8 bit.tiff image stacks to create a 'region of interest' (ROI) around the shell and its membrane. Using the 'porosity/inclusion volume analysis tool' the shell matrix, shell membrane and air spaces (pores) were isolated from one another based on grey-scale intensity, corresponding to the density of the specific feature. The thickness of the shell and the membrane as well as the volume of the shell matrix and pores were highlighted and measured.

2.2.6 | Analysis of quantitative data

The basic descriptive statistics were calculated for each subset of measurements (eggshell regions; A–E, within measurement data sets; pore count, mammillae count, eggshell thickness, membrane thickness, pore volume, shell volume and porosity); this included minimum, maximum, mean, median, standard deviation kurtosis and skewedness. A Jarque–Bera (JB) test was performed on each data subset (egg region within a measurement set) to test the assumption that the values in the data set are normally distributed.[38]

$$JB = \frac{n}{6}\left(S^2 + \frac{1}{4}(K-3)^2\right),$$

where n is number of observations, S is sample skewness and K is sample kurtosis.

If normal distribution was confirmed, a one-way analysis of variance (ANOVA) was conducted on each measurement data set (pore count, mammillae count, eggshell thickness, membrane thickness, pore volume, shell volume and porosity) to determine if there are any statistically significant differences between the different regions (A–E) of the eggshell. The probability of $p < 0.05$ was assumed to be statistically significant. If significant differences were indicated, follow-up paired t-tests were used between individual egg regions to locate the source of the difference. The probability of $p < 0.05$ was again assumed to be statistically significant. If the data subsets did not conform to normality the nonparametric Kruskal–Wallis test was used to determine statistically significant differences, followed by the Mann–Whitney U test to locate the differences.

TABLE 1 Macro eggshell parameters of the of the *C. niloticus* eggshell ($n = 50$).

Parameter	Min.	Max.	Mean	Std. dev.
Egg weight M (g)	97.49	149.44	120.01	12.21
Egg length L (mm)	65.59	92.11	79.83	5.31
Egg maximum width W (mm)	39.04	54.18	49.78	3.00
L to W ratio	1.39	1.99	1.61	0.12
Measured egg volume MV (cm^3)	90.00	141.00	110.68	13.17
Calculated egg volume V (cm^3)	54.10	133.69	107.54	15.09
Calculated surface area S (cm^3)	71.22	96.34	89.68	4.81

3 | RESULTS

3.1 | Macrostructural observations

C. niloticus eggs are translucent white and ellipsoidal in shape (Table 1) with an average length-to-width ratio of 1.61, and an average length, width and weight of 79.83 (SD = 5.31), 49.78 mm (SD = 3.00) and 120.01 g (SD = 12.21), respectively. Averages of calculated egg volumes and measured egg volume differs by ±3 cm^3 with calculated volume as the lowest at 107.54 cm^3; this discrepancy is not considered to be problematic as the water-displacement method, although providing a good estimation, is known to be an inconsistent measurement technique in porous objects.[39] The egg surface is calculated to be 89.68 cm^2 (SD = 4.81). All measured and calculated parameters show a relatively large range between minimum and maximum values, which is to be expected as the eggs used in this investigation were laid by different aged and sized females.

3.2 | Microstructural observations

The structure of the Nile crocodile's eggshell is divided into two basic layers, the outer calcified layer referred to as the shell and the inner organic fibre layer referred to as the shell membrane.

The shell consists of inorganic polycrystalline calcite measuring roughly 45 mm in thickness (Table 2, Figure 1A). Interestingly the thickness of the calcified shell was found not to be uniformly distributed equally over the egg regions. The thickest part of the shell is found on the equator of the egg, thinning off towards both the poles ($F_{4,116} = 4.878$, $p = 0.001$).

The calcified shell can be classified in three zones based on the organisation of the crystallographic and 'skeletal material' structure: the vertical crystal or external, the palisade or column and the mammillary layers. Polarised and differential interference light microscopy shows the

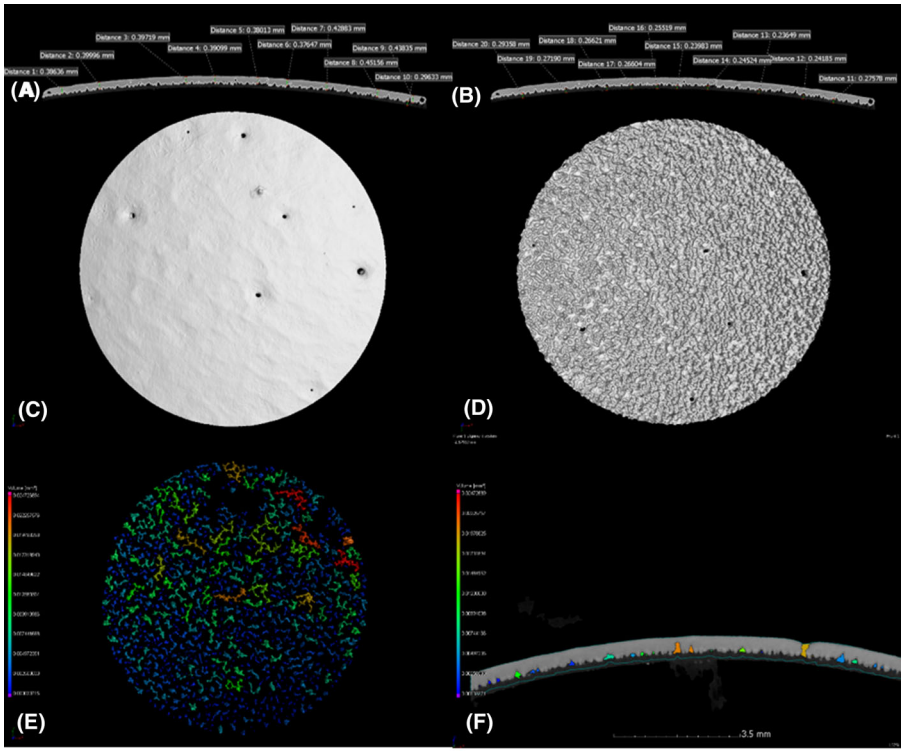

FIGURE 1 Micro-CT images. Eggshell and membrane transverse slice with measurements of the shell (A) and membrane (B). C: External surface view of the eggshell. D: Internal surface view of the eggshell. E: Airspaces and pore channels present in the eggshell and between the shell and the membrane, colour coded according to volume. F: Transverse slice of the eggshell and membrane with colour-coded airspaces and pore channels.

TABLE 2 The *C. niloticus* eggshell thickness (mm) in the different eggshell regions (A–E), as measured from micro-CT analysis (1 cm^2 disc) ($n = 15$).

	Min.	Max.	Mean	Std. dev.
A	3.07	5.64	4.24^{wz}	0.12
B	3.48	5.59	4.50	0.08
C	3.67	5.56	4.69^{x}	0.09
D	3.50	5.27	4.48^{y}	0.08
E	3.18	5.09	4.26^{wz}	0.11

Note: Different letter superscripts signify statistical differences ($p < 0.05$).

external layer as dark and light layers respectively with no discernable crystal structure (Figure 2). Scanning electron microscopy images of freshly fractured eggshells illustrates a thin external layer that is morphologically dissimilar to the underlying layer (Figure 3A and B), with a different fracture pattern compared to the palisade layer and which in some cases can be seen to detach from the underlying layer (Figure 3B). EBSD analysis of *C. niloticus* eggshell shows that the palisade layer ends in a fine serrated edge in what appears to be an epitaxial growth pattern (Figure 4) above which the external layer is located showing no observable crystal structure. This suggests that the external layer is not composed of a crystalline calcite, or not of calcite at all. Further EDS analysis shows that the external layer contains high concentrations of phosphorus deposits (Figure 5D), demonstrating that this layer primarily consists of a phosphorus and an amorphous form of calcite.

The palisade layer also sometimes called the column or honeycomb layer forms the largest part of the shell and is made up of large wedge or triangular-shaped shell units expanding towards to the eggshell surface (Figures 2A and 4B). Each shell unit is a single calcite crystal orientated with a *c*-axis perpendicular to the shell surface (Figure 4). The wedges vary in size and shape with rough and irregular boundaries attaching to one another laterally. The palisade layer shows a tabular ultrastructure with horizontal accretion lines or so-called growth lines, which can be observed throughout the entire layer (Figure 2B). Transmission electron microscopy of decalcified eggshells demonstrates a complex matrix architecture coexisting within the calcite mineral phase. Towards the outer eggshell boundary, this organic structure is arranged in elongated linear units running approximately parallel to the eggshell surface, changing to more squamatic-shaped units approaching the mammillary layer (Figures 6D and 7H).

The innermost mammillary layer is basal plate groups composed of rosette-like structures, which forms the

Journal of Microscopy RMS

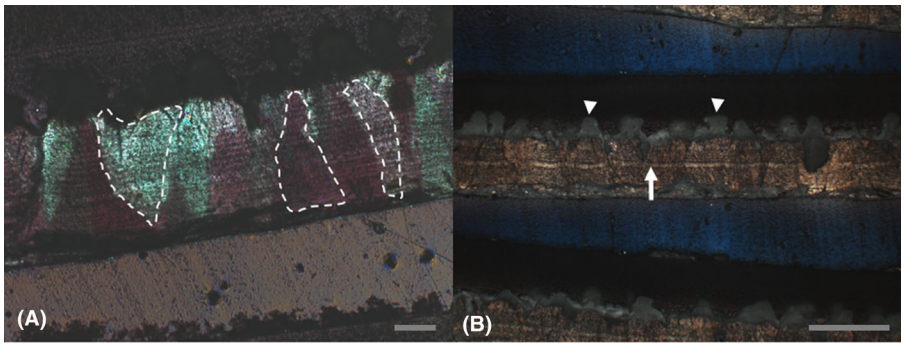

FIGURE 2 Optical microscopy images of radial thin sections of *C. niloticus* eggshell and membrane. A: Cross polarised light image showing the irregular wedge-shaped crystal structure (dashed border) of the palisade layer, scale bar = 100 μm. B: Differential interference contrast image showing the anisotropic characteristics, as deposition lines (arrows), and the lack of recognizable crystal structures in the mammillary layer (arrowheads) of the eggshell, scale bar = 200 μm.

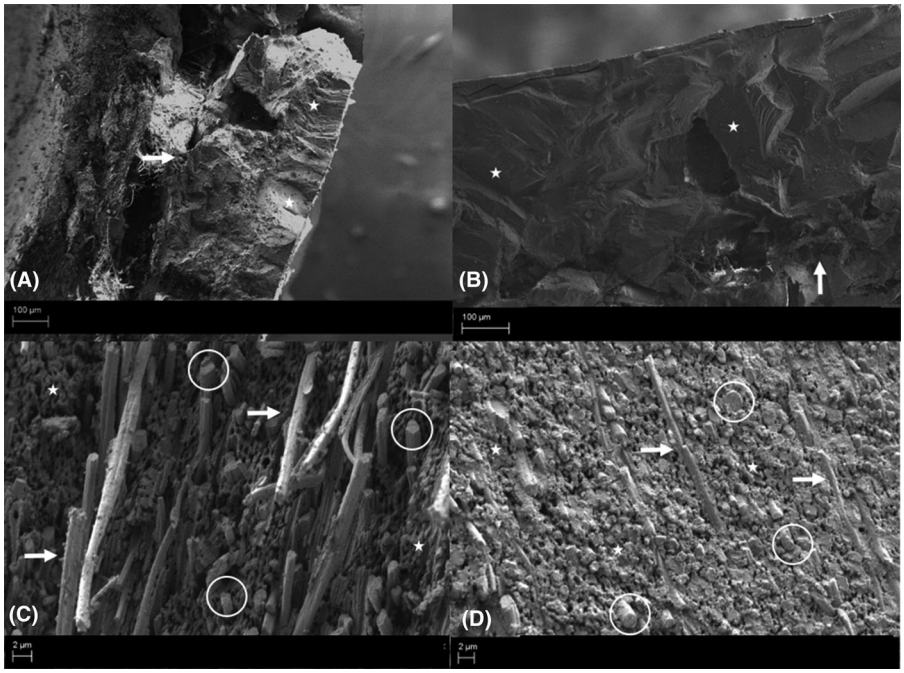

FIGURE 3 Scanning electron microscopy images of the transverse view of the eggshell and the eggshell membrane. A: Transverse view of the eggshell prepared by scalpel dissection showing the shell-membrane attachment (arrow) and the fracture planes (stars), scale bar = 100 μm. B: Transverse view of the eggshell prepared by freeze fracture showing the shell-membrane attachment (arrow) and the fracture planes (stars), scale bar = 100 μm. C: Transverse view of the eggshell membrane prepared by scalpel dissection showing fibres arranged longitudinally (arrows) and transversely (circled) between the matrix (stars), scale bar = 2 μm. D: Transverse view of the eggshell membrane prepared by wax embedding, sectioning and de-waxing showing fibres arranged longitudinally (arrows) and transversely (circled) between the matrix (stars), scale bar = 2 μm.

bulbous base of the shell units (Figures 4B and 8B). The basal plate groups or mammillary knobs are relatively densely arranged (although less so than what is observed in avian eggshells) with no discernible organisational order (Figures 1D and 9). The number of mammillary knobs is not equally distributed over egg regions (Table 3), with the highest number of knobs seen on the equator of the egg, declining in number towards the egg poles ($F_{4,\,24}$ = 18.210, $p = 5.384 \times 10^{-7}$). Scanning electron microscopy shows the mammillary knobs to be relatively uniform sized mounds with an uneven surface composed of spherulitic microcrystals (Figure 8B). Neither polarised nor differential interference contrast microscopy of the mammillary layer shows any birefringence; the layer presents as uniform dark or white areas respectively (Figure 2). This observation does not indicate that the layer is

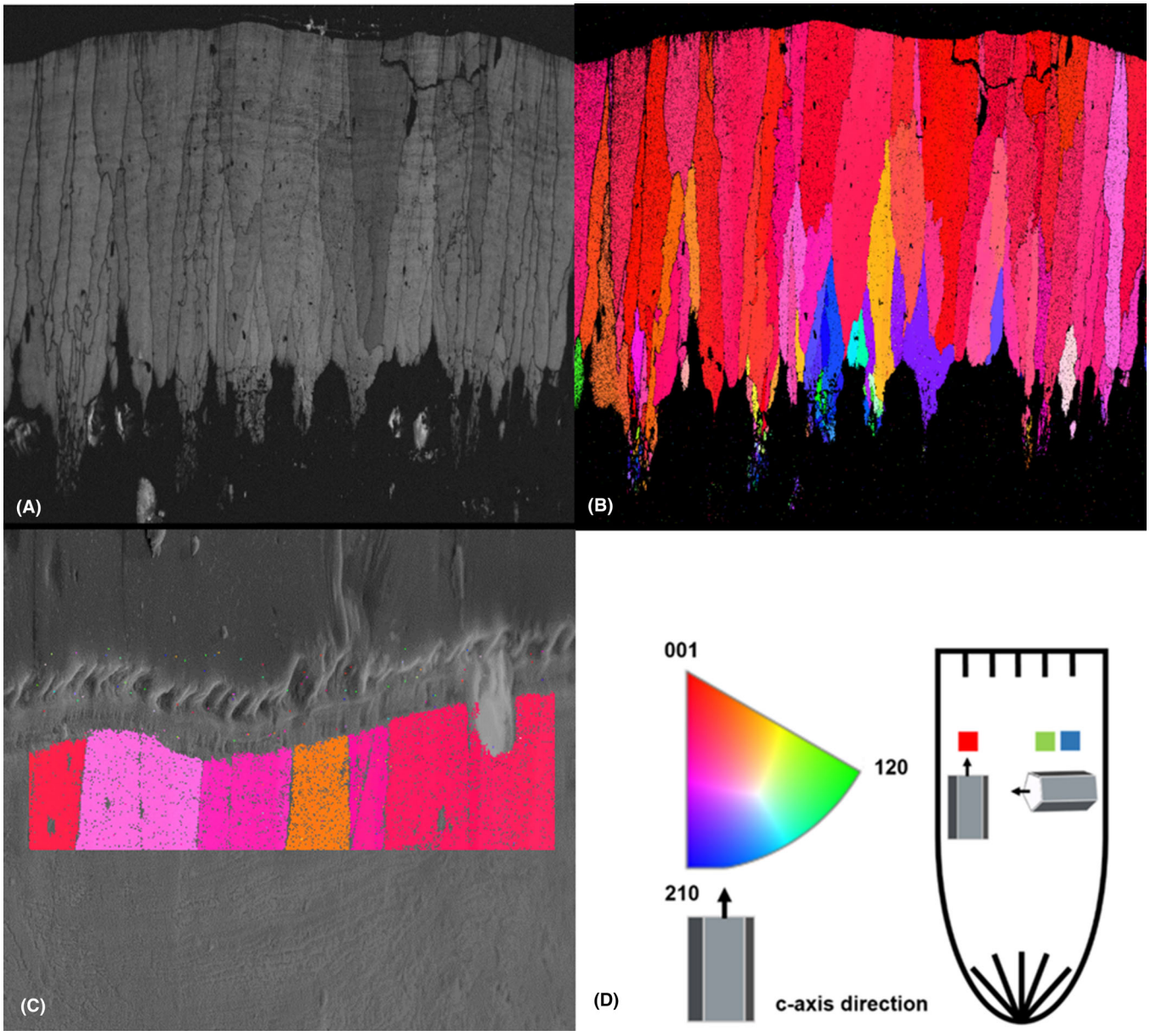

FIGURE 4 EBSD orientation maps of radially sectioned and polished eggshell. A: Diffraction intensity map showing the structure and grain boundaries of the crystals. B: Inverse pole figure (IPF) map (reference direction X) showing the structure, grain boundaries and orientation of the crystals. C: Secondary electron image overlaid with matching EBSD IPF map (reference direction X) showing the structure, grain boundaries and orientation of the crystal composition of the outer part of the palisade layer and the lack of crystal structure in the external layer of eggshell. D: Corresponding inverse pole figure and schematic crystal orientation description.

TABLE 3 The number of mammillary knobs found in each eggshell region (A–E), as counted from stereo microscopy images of the *C. niloticus* eggshell.

	Min.	Max.	Mean	St. dev.
A	106	194	139.00^{w}	32.91
B	124	241	173.86^{xz}	37.18
C	134	288	206.71^{y}	53.80
D	105	243	177.43^{xz}	50.62
E	101	213	142.71^{w}	36.18

Note: Different letter superscripts signify statistical differences ($p < 0.05$).

noncrystalline, but rather that the lack of discernible anisotropic characteristics is due to the resolution capability inherent to light microscopes. EBSD analysis which has much higher resolution power demonstrates the crystal structure of the mammillae clearly (Figure 4B). The crystal structure and grain size of this layer is considerably smaller than the crystal structures of the overlaying layer, with randomly orientated crystals. The boundary between the mammillary and palisade layers is irregular, with the shell units from the palisade layer appearing to initiate from the mammillary layer and continue towards the exterior

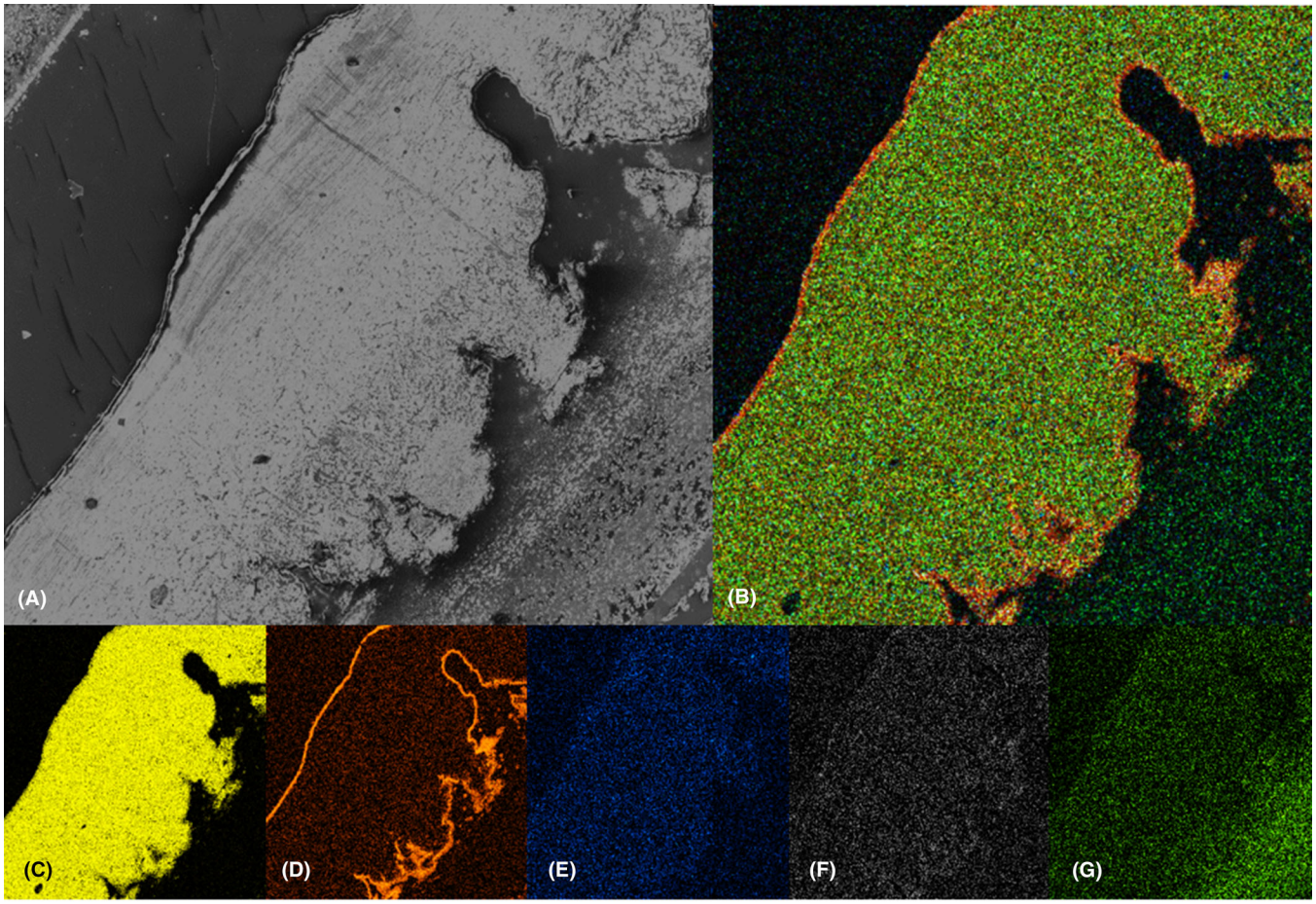

FIGURE 5 EDS compositional maps of the eggshell. A: Secondary electron image of the area of analysis. B: Combined elemental map of the elements identified in the eggshell. C–G: Individual element maps. C: Calcium. D: Phosphorus. E: Magnesium. F: Sodium. G: Sulphur.

of the shell. Decalcified eggshells imaged by transmission electron microscopy show a fine matrix architecture with irregularly shaped units in and through which fibres from the eggshell membrane are embedded (Figures 6A, B, D and 7G–H). Both the palisade and the mammillary layers are composed of calcium with traces of magnesium, sodium, sulphur and phosphorus (Figure 5).

Between the bases of the mammillary knobs' airspaces exist (Figure 1E and F), occasionally these airspaces form a pore canal that spans from the inner surface of shell (mammillary layer) to the outermost surface of the shell (Figures 1C, E and F and 8A). The pattern observed in the pore distribution matches the distribution pattern found in the mammillae (Table 4), with the highest number of pores seen on the equator of the egg, declining in number towards the poles of the egg, although these observed differences were not significant. Micro-CT measurements of the shell volume (Table 5) pore volume (Table 6), pore surface area (Table 7) and the porosity (pore percentage) (Table 8) shows a similar pattern. The difference in pore volume ($F_{4,8} = 10.170$, $p = 0.003$), pore surface area ($F_{4,8} = 4.054$, $p = 0.043$) and porosity ($F_{4,8} = 16.361$, $p = 6.426 \times 10^{-4}$) was found to be significantly different between the eggshell regions. The pore channels are relatively straight, unbranched and, in most instances, the round outermost opening is smaller in size than the end opening between the mammillary knobs (Figures 1A, 8A and 10). This type of pore system is classified as an angusticanaliculate[5] pore system. High-magnification scanning electron images of a mould of the pores show the pores to have circumferential grooves giving the boundary a layered appearance (Figures 10B). These grooves or layering correspond to the horizontal accretion lines seen

TABLE 4 The number of eggshell pores found in each eggshell region (A–E), as counted and normalized for the shell fragment size of the *C. niloticus* eggshell.

	Min.	Max.	Mean	Std. dev.
A	5	23	13.60	7.83
B	9	28	15.00	7.78
C	12	33	18.20	8.58
D	9	17	12.00	3.32
E	3	23	11.80	8.17

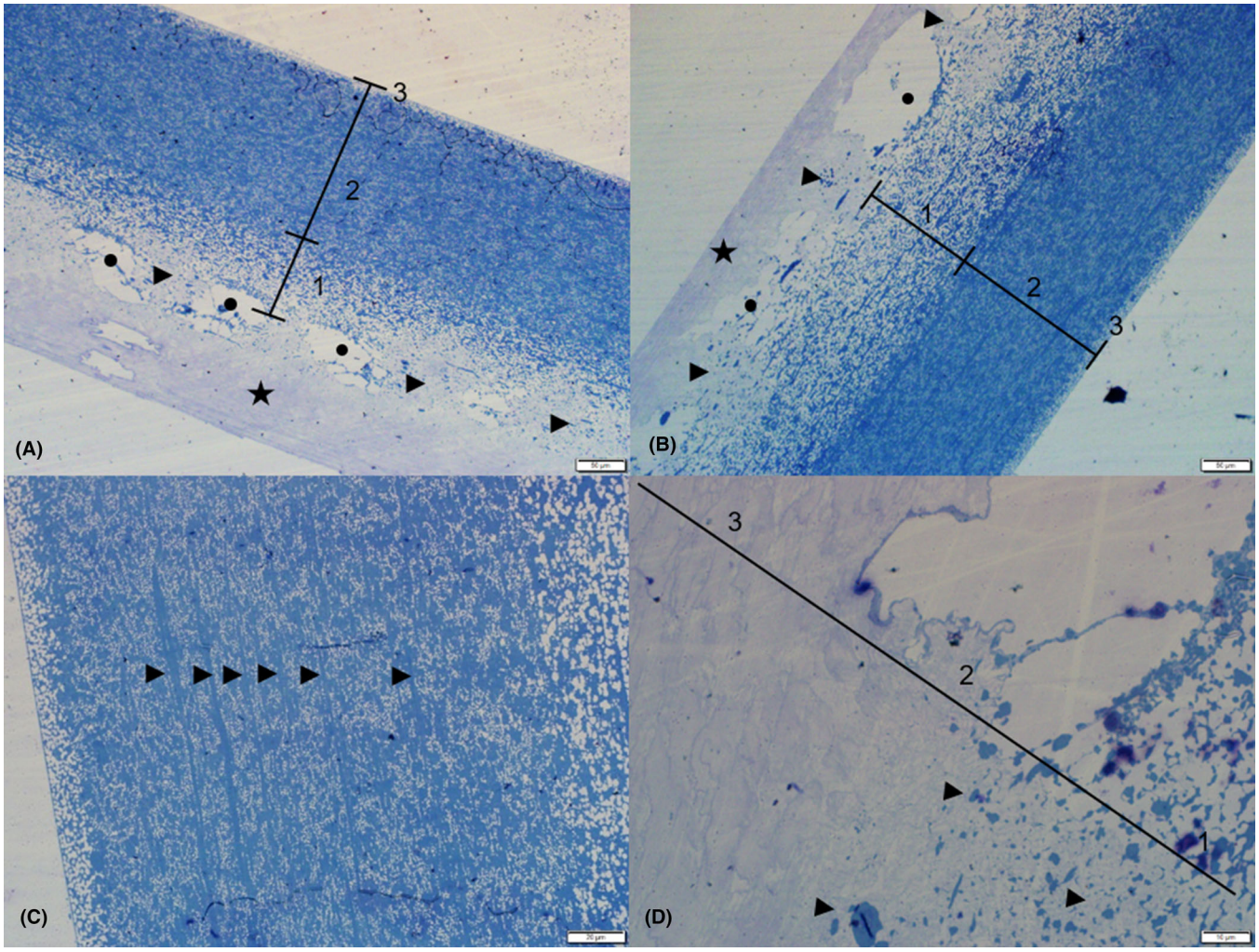

FIGURE 6 Transmitted light microscopy images of semithin sections from epoxy resin embedded toluidine blue-stained eggshell membrane. A, B: Low magnification image of the decalcified eggshell (star) and eggshell membranes, showing the shell-membrane connection points (arrowheads), airspaces (dots) and different areas of the membrane (large loosely packed fibres (1), smaller densely packed fibres (2) and limiting membrane (3), scale bar = 50 μm. C: Higher magnification image showing the sheet arrangement of the membrane fibres (longitudinal sheets illustrated with arrows), scale bar = 20 μm. D: High-magnification image showing the membranes embedded in the shell (arrowheads) at the shell-membrane connection point, and the change of the shell matrix ultrastructure from the mammillary knobs towards the palisade layer (1 to 3) from smaller squamatic to larger elongated units, scale bar = 10 μm.

TABLE 5 The *C. niloticus* eggshell volume (mm^3) in the different eggshell sections (A–E), as measured from a 1 cm^2 disc by micro-CT analysis ($n = 15$).

	Min.	Max.	Mean	Std. dev.
A	39.65	45.18	45.51	5.15
B	41.30	48.58	44.74	3.20
C	44.26	48.69	47.82	4.02
D	46.78	48.96	48.26	1.35
E	42.02	47.88	44.77	2.46

TABLE 6 The *C. niloticus* pore volume (mm^3) in the different eggshell sections (A–E), as measured from a 1 cm^2 disc by micro-CT analysis.

	Min.	Max.	Mean	Std. dev.
A	0.15	0.66	0.49^{x}	0.30
B	0.71	1.64	1.26^{y}	0.47
C	1.00	2.59	$1.69^{y,z}$	0.81
D	0.98	1.62	$1.19^{y,x}$	0.37
E	0.08	0.75	0.35^{x}	0.35

Note: Different letter superscripts signify statistical differences ($p < 0.05$).

with differential light microscopy (Figure 2B). Nano-CT analyses shows that the body of the inorganic shell also contains nano-pores. These pores only occupy 0.06% of the total volume, are concentrated closer to the inner surface (Figure 11), have average diameters between 10 and 30 μm and an average sphericity of 0.5.

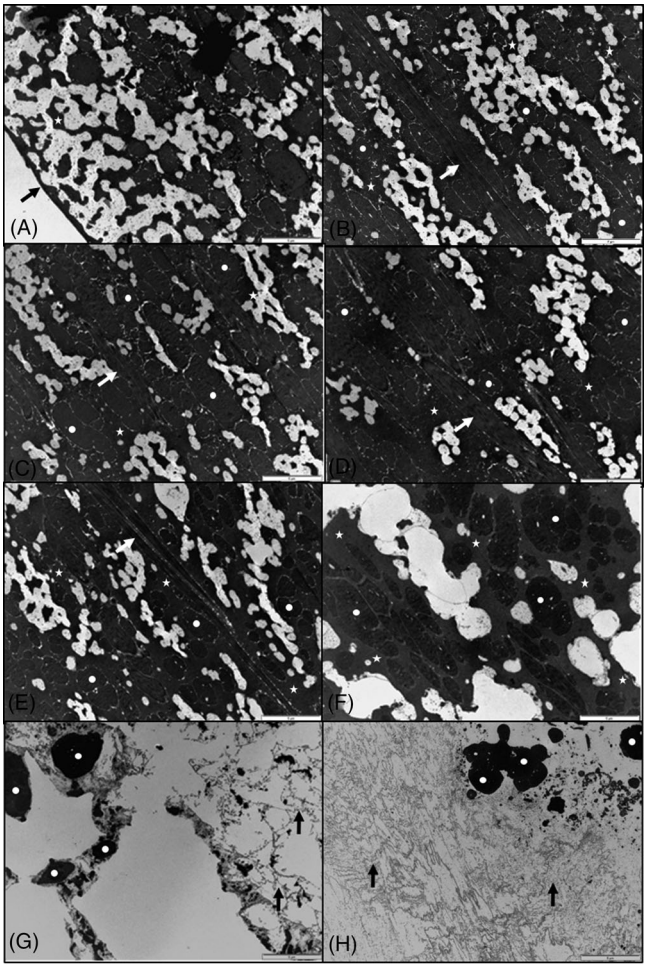

FIGURE 7 Transmission electron microscopy image series of the eggshell membrane and decalcified eggshell of the *C. niloticus* egg. A is representing the innermost part of the membrane and H the outermost part of the sample. A: Limiting membrane (arrow) with an area containing matrix, but no fibres (star). B–E: Mid-membrane with densely packed fibres cut longitudinally (arrows) and transversely (dots) with matrix between the fibres (stars). F–H: Outer membrane with large loosely arranged fibres cut transversely (dots) with matrix between the fibres (stars) and decalcified shell (arrows). A, C, D, E, F and E: scale bar = 1 μm. B and H: scale bar = 5 μm.

TABLE 7 *C. niloticus* pore surface areas (mm^2) in the different eggshell regions (A–E), as measured from a 1 cm^2 disc by micro-CT analysis ($n = 15$).

	Min.	Max.	Mean	Std. dev.
A	16.44	53.29	39.12^{y}	19.84
B	59.44	66.50	62.15	3.81
C	61.33	91.33	78.24^{z}	15.36
D	43.58	46.21	45.33^{y}	1.52
E	10.98	77.41	38.59	34.61

Note: Different letter superscripts signify statistical differences ($p < 0.05$).

TABLE 8 *C. niloticus* eggshell porosity (pore percentage) (%) values in the different eggshell regions (A–E) as calculated from micro-CT shell and pore volume measurements ($n = 15$).

	Min.	Max.	Mean	Std. dev.
A	0.38	1.38	1.02^{x}	0.56
B	1.55	3.53	2.74^{y}	1.05
C	2.84	3.68	$3.20^{y, z}$	0.44
D	1.99	3.16	$2.40^{x, y, z}$	0.66
E	0.20	1.57	0.76^{x}	0.72

Note: Different letter superscripts signify statistical differences ($p < 0.05$).

TABLE 9 The *C. niloticus* eggshell membrane thickness (mm) in the different eggshell regions (A–E), as measured from micro-CT analysis (1 cm^2 disc) ($n = 15$).

	Min.	Max.	Mean	Std. dev.
A	1.89	3.73	$2.79^{V, W}$	0.54
B	2.27	3.83	2.96^{W}	0.33
C	2.65	4.38	3.24^{X}	0.32
D	2.09	3.76	$3.06^{W, X, Y, Z}$	0.41
E	2.22	4.32	$3.16^{X, Z}$	0.59

Note: Different letter superscripts signify statistical differences ($p < 0.05$).

Right beneath and embedded in the mammillary layer the eggshell membrane is found (Figures 6 and 8B–D). The average membrane thickness was measured to be approximately 3.06 mm (SD = 0.44) (Figure 1B), with statistically different thicknesses found between the regions of the shell ($\chi^2(4, N = 150) = 14.073$, $p = 0.006$). Interestingly, statistical differences were most pronounced at the pole that also has the highest number of mammillae, pores, porosity and pore surface area when compared to the rest of egg. (Table 9). All fibres are orientated parallel to the shell surface and arranged in sheets at relatively right angles to one another (Figures 3C–D, 6 and 7A–E). The number and thickness of these sheets vary between eggs. This arrangement is believed to be due to the egg movement and rotation during fibre deposition in the oviduct of the female crocodile. Although no clear distinction of different fibre layers is observable, generally, the outermost fibres are larger with large inter-fibrillary spaces; the mid-region of the membrane is dense with smaller fibres and the innermost isolating boundary is a thin single layer (called the limiting membrane). Measurements of individual fibre diameters class the fibres into three approximate layers, which correlate to the density arrangement mentioned above, and further subdivided into zones (Table 10, Figure 7). The outermost layer is comprised of fibres embedded in the shell matrix, classed as zone 1 (Figure 7G and H), and fibres immediately underneath the shell loosely arranged with abundant matrix substance in between, classed as

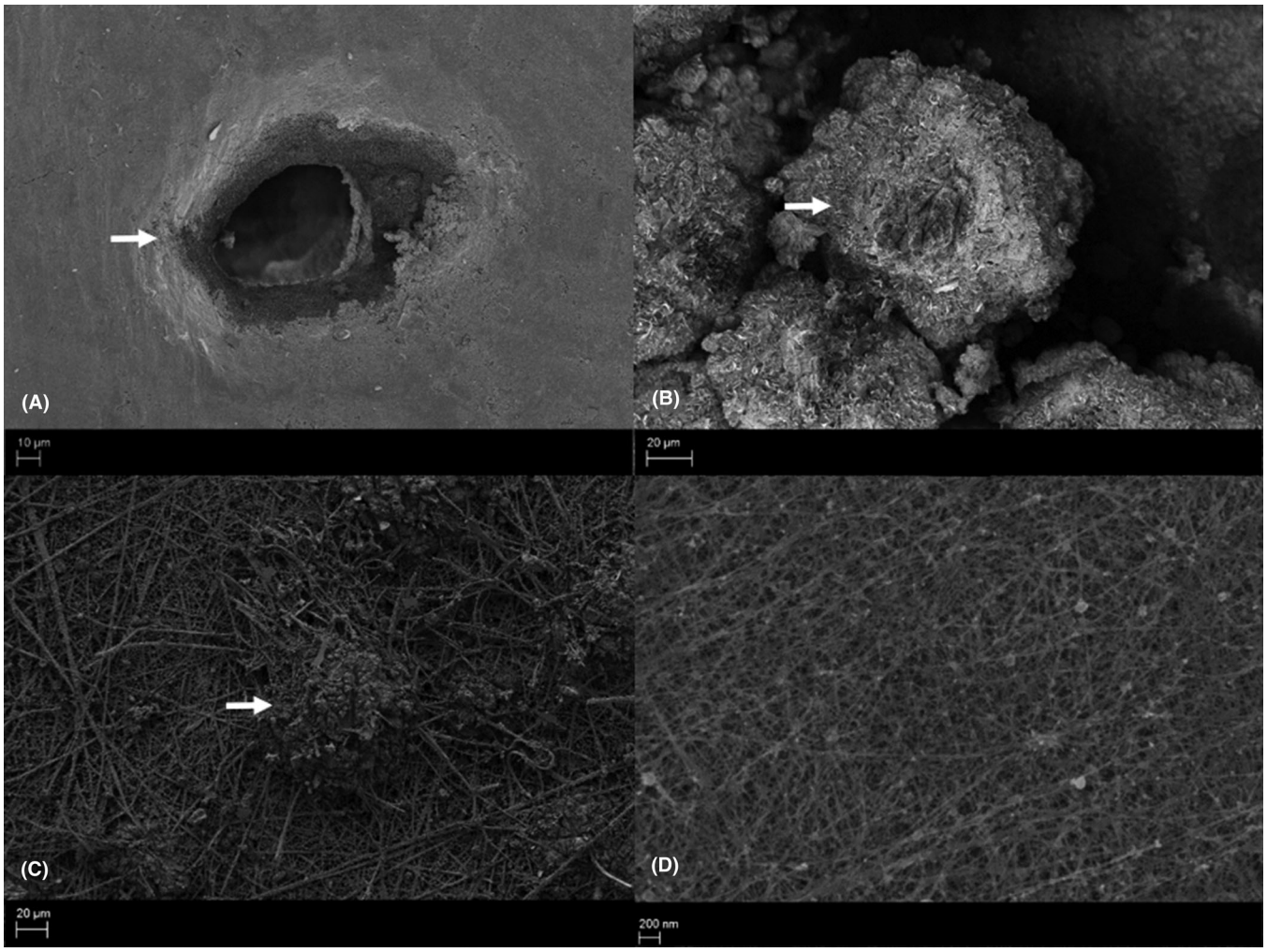

FIGURE 8 Scanning electron microscopy images of the eggshell and the eggshell membrane. A: External shell surface view of a pore channel opening (arrow), scale bar = 10 µm. B: Internal shell surface view of a cleaned mammillae (arrow), scale bar = 20 µm. C: Internal shell surface view of a mammillae with embedded membrane fibres (arrow), scale bar = 20 µm. D: Membrane fibres, scale bar = 200 nm.

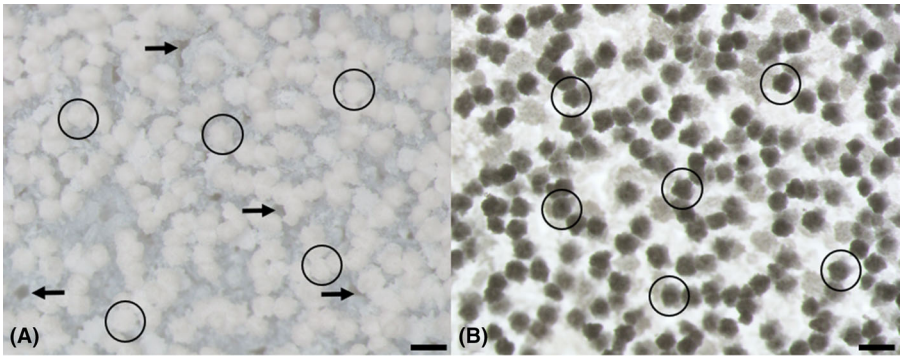

FIGURE 9 Stereo microscopy images of the mammillae (circled) and eggshell pores (arrows) on the interior surface of the eggshell. A: Reflected illumination, scale bar = 200 µm. B: Transmitted illumination, scale bar = 200 µm.

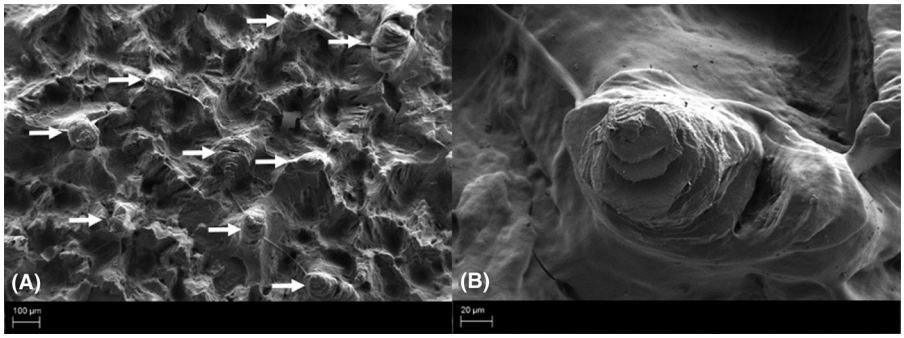

FIGURE 10 Scanning electron microscopy image of epoxy resin moulds of the pore channels and interior surface of the eggshell. A: Low-magnification image showing several eggshell pores (arrows), scale bar = 100 µm. B: High-magnification image of a single pore channel, scale bar = 20 µm.

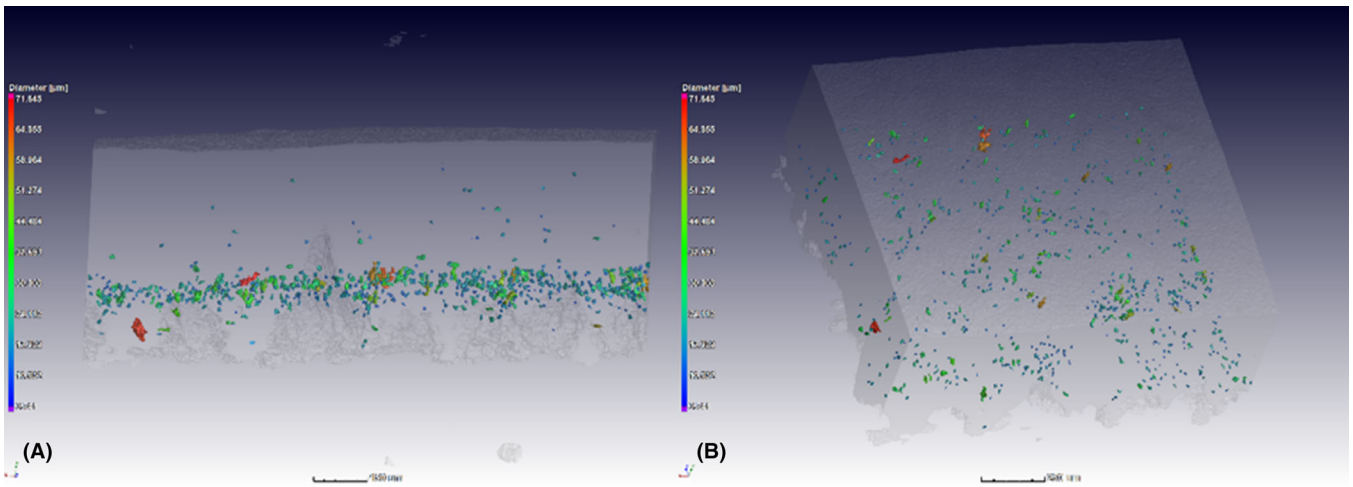

FIGURE 11 Nano-CT images of the internal porosity in the eggshell, colour-coded according to volume. A: Transverse view. B: Oblique view.

TABLE 10 The *C. niloticus* eggshell membrane fibre size (µm) measured in the different parts of the membrane using TEM images ($n = 6$).

Layer	Zone	Min.	Max.	Mean	Std. dev.
1	1	0.70	5.55	1.52	0.99
	2	0.30	5.15	1.06	0.92
	(1+2)	0.30	5.55	1.26^{x}	0.98
2	3	0.20	3.62	0.96	0.59
	4	0.16	3.62	0.85	0.47
	5	0.16	3.49	0.87	0.46
	6	0.29	3.48	1.22	0.66
	(3+4+5+6)	0.16	3.62	0.90^{y}	0.53
3	7	0.32	0.41	0.35^{z}	0.03

Note: Different letter superscripts signify statistical differences ($p < 0.05$).

zone 2 (Figure 7F). Layer ones' fibres have an average diameter larger than 1 micrometre (minimum 0.3 µm, maximum 5.5 µm). The middle layers' fibres were found to have approximate diameters between 0.8 and 0.9 micrometres (minimum 0.1 µm, maximum 3.6 µm). This layer is further divided into four zones the first of which is loosely arranged smaller fibres (Figure 7E) and the second and third layers are sequential zones of densely packed smaller fibres only moderately distinguishable by the density of the fibres and the amount of matrix found between the fibres (Figure 7C and D). The fourth zone in the middle layer is composed a loosely arranged zone of fibres found right above the limiting membrane (Figure 7B). The innermost layer or the so-called limiting membrane is roughly 0.3 micrometres (minimum 0.2 µm, maximum 0.4 µm) (Figure 7A). The differences in the fibre diameters between the three main layers were found to be statistically significant ($F_{2,\ 3634} = 1019.914$, $p < 0.0001$) (Table 10). Transmission electron microscopy shows that the fibres are round to oval shaped, although in many instances it appears that fibres combine or closely associated with one another to form more pleomorphic forms. Individual

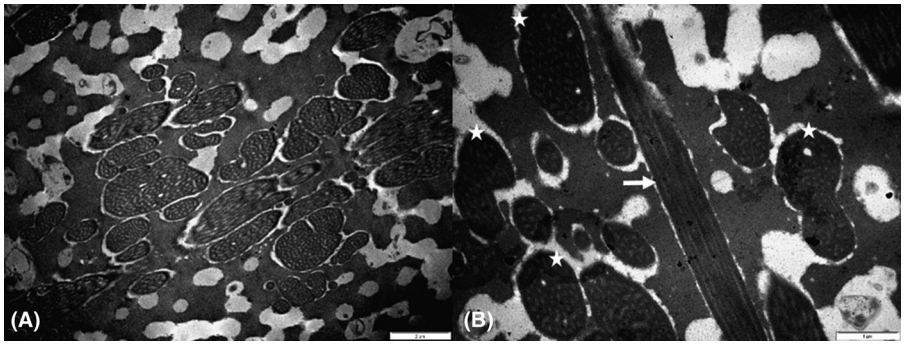

FIGURE 12 Transmission electron microscopy images of eggshell membrane fibres. A: Transversely sectioned fibres, scale bar = 2 μm. B: Transversely (stars) and longitudinally (arrows) sectioned fibres, scale bar = 1 μm.

fibres are made up of numerous smaller fibrils forming hollow channels that run longitudinally through the fibre length (Figure 12). In transverse sections, the arrangement of channels can be seen to form a circular pattern (Figure 12).

4 | DISCUSSION AND CONCLUSION

The crocodile egg structure needs to meet several requirements to fulfil its function as an effective incubation unit for successful embryonic development and, ultimately, the continuation of the species. The egg must be strong enough to withstand the initial mechanical stress and strain of egg laying and the subsequent nest closure and compaction by the adult female. After this, it needs to allow for gas exchange while preventing dehydration, supply the necessary minerals for embryo development and protect against invasion of microorganisms such as bacterial and fungal agents.[1,2,3,4] The macro- and ultrastructures of the egg are remarkably suitable to fulfil these specific needs. Although round-shaped eggs have been shown to have higher shell breaking strength and stability in avian eggs,[40,41] the greater thickness of the ellipsoid *C. niloticus* eggshell, optimally shaped for the dimensions of a growing crocodile embryo especially around the equator, is hypothesised to compensate for a geometrically weaker shape. The vertical alignment of the *c*-axis of the wedge-shaped crystals in the palisade layer together with the rugged grain boundaries imparts strength to the shell. Although a certain ordered distribution in the number of mammillae and pores were observed over the egg as a whole, the placement of these structures is not systematic which has been shown to be the best suited distribution for strength and robustness. The arrangement of the membrane fibres does not seem to predict where the inorganic seeding of the shell will start, but embedment of fibres into the mammillae anchors the two protective layers of the egg together. The air spaces between shell and membrane aid in permeability for gas and fluid exchange and allow for a certain amount of swelling to occur without compromising the developing embryo. This is possibly further aided by the 'hollow' fibres that would impart additional elasticity and strength, as well as thermal insulation. Guillette et al.[28] suggested that this type of arrangement might also be a mechanism to reduce the amount of protein invested in the membrane during the formation process. The layering of the stronger thick loose fibres and smaller densely packed fibres is optimal for protection from the penetration of microorganisms.

The existence of air spaces in reptile eggs has been controversially reported and consequently debated in literature. Numerous studies[8,42,43,44] reported that no airspaces existed in the alligator egg. These studies suggested that the airspaces observed between the eggshell and outer membrane of reptile eggs by several other authors[16,45,46,47,48] were probably artefacts due to dehydration. Although this study was conducted on crocodile eggs and not American alligator eggs as with the case in the majority of the other studies, the results using several different investigation techniques and preparation methods showed very clear airspaces between the membrane and the inner aspect of the eggshell. These air spaces are completely unlike the 'air cell' observed in avian eggs, which is a large prominent air-filled space between the inner and outer eggshell membrane on the blunt pole of the egg. The air cells function is mainly for the facilitation of the hatching process and the subsequent initiation of pulmonary respiration. The air spaces in the *C. niloticus* egg are small spaces found on the inner aspect of the eggshell, between the eggshell and the eggshell membrane. The spaces are often largest at the base of eggshell pores.

The distribution and presence of mammillary knobs or mammillae have also been reported contrarily; some studies reported that mammillary knobs were far more distinct and numerous in the central region,[42] whereas others reported a complete absence of mammillae.[5] In the present study, it was found that the highest

number of mammillae can be found on the central equator of the egg, although this investigator would not describe the difference in number as 'much more numerous' as Ferguson[42] reported. Also, the knobs observed on the poles of the egg were no different in morphology, less distinct, or had a reduced membrane-mammillae connection than the knobs on the egg equator. Comparison between the different egg regions showed the same trend in the number of pores, with the highest number found in the central region of the egg. Although these differences were not statistically significant, we believed that it is due to the low number of samples evaluated ($n = 6$ per region), coupled with the natural high variability as observed in most biological samples. Even without statistically significant differences in the light microscopy counts, significant differences were detected between regions in micro-CT pore volume, surface area and percentage analysis, which support the observed trend. As with the regional differences in mammillary knob and pore counts, the membrane and eggshell have consistent variability in thickness across different egg regions, with the thickest area found around the equator of the egg. This has not been reported previously in the crocodilian species. Interestingly, all these measurements showed that one of the egg poles (region A) has consistently larger values of pore counts, pore volume, surface area and porosity and lower values of membrane thickness and mammillae counts. This could indicate a possible alteration in the shell strength on one side, which would aid the hatchling from exiting the egg, making this the 'hatching' pole of the egg.

Furthermore, previous studies on crocodylomorpha eggshells from other species reported that the external layer was a distinct layer of vertically stacked rhombohedral-shaped crystals.[42] This investigation found the external layer to mainly consist of calcium and phosphorus in an amorphous form without any crystalline structure.

Additionally, this study highlights the importance of using different complimentary microscopic analytical and imaging techniques when investigating and comprehensively describing composite micro- or macroscopic samples. This is especially true with samples comprised of elements with organic–inorganic interfaces, which inherently spans cross-disciplinary study fields with reference to microscopy. For example, the *C. niloticus* egg investigated in this paper is composed of a crystalline calcite shell and an associated collagenous fibrous membrane which could be affiliated with several fields of scientific study, for example, crystallography optical physics, organic chemistry, histology and structural biology. The similar use of several complimentary microscopy techniques could potentially add value to the studies of other types of composite samples, such as biological structures (bone and teeth), matrix composites (polymeric and metallic), nanobiohybrids and bioceramics, to name a few.

ACKNOWLEDGEMENTS

We as authors thank all the participating crocodile farms for provision of sample material and assistance during data collection. Furthermore, we acknowledge the following people and organisations/facilities for their contribution towards our research: the beam line scientists of the RADTOM section, EJ Hoffman and LC Bam, as well as the DST-NRF for the financial support (Grant # UID23456) to establish the MIXRAD microfocus X-ray tomography facility at Necsa; The Electron Microscope Unit, Department of Anatomy and Physiology, Faculty of Veterinary Sciences and the Microscopy and Microanalysis Laboratory, Department of Physics, Faculty of Natural and Agricultural Sciences from the University of Pretoria for the use of your light and electron microscopy equipment. Funding for this research was provided by HWSETA in the form of a postgraduate bursary and the IUCN-SSC Crocodile Specialist Group in the form of a grant (SRAS Project (18/08)).

CONFLICT OF INTEREST STATEMENT

The authors have no conflicts of interest to declare.

ORCID

A V Lensink https://orcid.org/0000-0002-5206-3877

REFERENCES

1. Board, R. G. (1982). Properties of avian egg shells and their adaptive value. *Biological Reviews*, *57*, 1–28.
2. Kohring, R. R. (1999). Calcified shell membranes in fossil vertebrate eggshell: Evidence for preburial diagenesis. *Journal of Vertebrate Paleontology*, *19*(4), 723–727.
3. Nys, Y., Gautron, J., Garcia-Ruiz, J. M., & Hincke, M. T. (2004). Avian eggshell mineralization: biochemical and functional characterization of matrix proteins. *Comptes Rendus Palevol*, *3*(6-7), 549–562.
4. Packard, M. J., & DeMarco, V. G. (1991). Eggshell structure and formation in eggs of oviparous reptiles. In D. C. Deeming & M. W. J. Ferguson (Eds.), *Egg incubation: Its effects on embryonic development in birds and reptiles* (pp. 53–69). Cambridge: Cambridge University Press.
5. Erben, H. K. (1970). Ultrastrukturen und mineralisation rezenter und fossiler Eischalen bei Vogeln und Reptilien. Germany: Schattauer.
6. Hirsch, K. F. (1983). Contemporary and fossil chelonian eggshells. *Copeia*, *1983*(2), 382–397.
7. Hirsch, K. F. (1996). Parataxonomic classification of fossil chelonian and gecko eggs. *Journal of Vertebrate Paleontology*, *16*(4), 752–762.
8. Packard, G. C., Tracy, C. R, & Roth, J. J. (1977). The physiological ecology of reptilian eggs and embryos. and the evolution of viviparity within the class reptilia. *Biological Reviews*, *52*(1), 71–105.

9. Packard, M. J., Packard, G. C., & Boardman, T. J. (1982). Structure of eggshells and water relations of reptilian eggs. *Herpetologica*, *38*(1), 136–155.
10. Hirsch, K. F. (1994). The fossil record of vertebrate eggs. In S. Donovan (Ed.), *The palaeobiology of trace fossils* (pp. 269–294). London: John Wiley & Sons.
11. Hirsch, K. F. (1985). Fossil crocodilian eggs from the Eocene of Colorado. *Journal of Paleontology*, *59*(3), 531–542.
12. Hirsch, K. F., & Quinn, B. (1990). Eggs and eggshell fragments from the Upper Cretaceous two medicine formation of Montana. *Journal of Vertebrate Paleontology*, *10*, 491–511.
13. Mikhailov, K. E. (1991). Classification of fossil eggshells of amniotic vertebrates. *Acta Palaeontologica Polonica*, *36*, 193–238.
14. Narushin, V. G., & Romanov, M. N. (2002). Egg physical characteristics and hatchability. *Worlds Poultry Science Journal*, *58*, 297–303.
15. Rossi, M., Nys, Y., Anton, M., Bain, M., De Ketelaere, B., De Reu, K., … Sirri, F. (2013). Developments in understanding and assessment of egg and egg product quality over the last century. *Worlds Poultry Science Journal*, *69*, 414–429.
16. Young, J. D. (2009). The structure and some physical properties of the testudinian eggshell. *Proceedings of the Zoological Society of London*, *120*, 455–469.
17. Maritz, M. F., & Douglas, R. M. (1994). Shape quantization and the estimation of volume and surface area of reptile eggs. *Journal of Herpetology*, *28*(3), 281–291.
18. Bain, M. M. (1992). Eggshell strength: A relationship between the mechanism of failure and the ultrastructural organisation of the mammillary layer. *British Poultry Science*, *33*, 303–319.
19. Checa, A G., Bonarski, J T., Willinger, M G., Faryna, M., Berent, K., Kania, B., … Morawiec, A. (2013). Crystallographic orientation inhomogeneity and crystal splitting in biogenic calcite. *Journal of The Royal Society Interface*, *10*, 20130425.
20. Rodriguez-Navarro, A., Kalin, O., Nys, Y., & Garcia-Ruiz, J. M. (2002). Influence of the microstructure on the shell strength of eggs laid by hens of different ages. *British Poultry Science*, *43*, 395–403.
21. Wink, C. S., Elsey, R. M., & Bouvier, M. (1990). The relationship of pores and mammillae on the inner surface of the eggshell of the alligator (*Alligator mississippiensis*). *Journal of Morphology*, *204*, 227–233.
22. Tyler, C. (1995). Studies on eggshells. VI. The distribution of pores in eggshells. *Journal of the Science of Food and Agriculture*, *6*, 170–176.
23. Wangensteen, O. D, Wilson, D., & Rahn, H. (1970). Diffusion of gases across the shell of the hen's egg. *Respiration Physiology*, *11*, 16–30.
24. Tullett, S. G, & Burton, F. G. (1985). The effects of eggshell porosity on blood-gas and acid-base status of domestic fowl embryos within eggs of the same weight. *Comparative Biochemistry and Physiology*, *181*, 137–142.
25. Kriesten, K. (1975). Untersuchungen fiber Ultra- struktur, Proteinmuster, und Aminosiiurenzusam – mensetzung der Eischalen von Testudo elephantopus, Caiman crocodilus und Iguana. *Zoologische Jahrbücher*, *94*, 101–122.
26. Sexton, O. J., Veith, G. M., & Phillips, D. M. (1979). Ultrastructure of the eggshell of two species of anoline lizards. *Journal of Experimental Zoology*, *207*, 227–236.
27. Trauth, S. E., Mcallister, C. T., & Chen, W. (1994). Microscopic eggshell characteristics in the collared lizard *Crotaphytus collaris* (Sauria: Crotaphytidae). *The Southwestern Naturalist*, *39*(1), 45–52.
28. Guillette, L. J., Fox, S. L., & Palmer, B D. (1989). Oviductal morphology and egg shelling in the oviparous lizards *Crotaphytus collaris* and *Eumeces obsoletus*. *Journal of Morphology*, *201*, 145–159.
29. Solomon, S. E., & Tippett, R. (1983). The diversity of crystal structure within the eggshells of the class Reptilia. *Journal of Anatomy*, *136*(3), 603–643.
30. Fergusson, R. A. (2010). *Nile Crocodile* Crocodylus niloticus. In Crocodiles. Status Survey and Conservation Action Plan (3rd edn., pp. 84–89). Crocodile Specialist Group: Darwin.
31. Ross, C. A., & Magnusson, W. E. (1990). Living crocodilians. In C. A. Ross (Ed.), *Crocodiles and alligators* (pp. 58–73). London: Merehurst Press.
32. Ross, J. P. (1998). Crocodiles. Status survey and conservation action plan. IUCN/SSC Crocodile Specialist Group.
33. Isberg, S. R., McLeod, R., & Ross, P. (2016). Crocodylus niloticus Red List workshop report. Report to the Steering Committee of the 24th Working Meeting of the IUCN-SSC Crocodile Specialist Group.
34. King, F. W. (1988). Crocodiles: Keystone wetland species. Wildlife in the Everglades and Latin American wetlands. G. H. Dalyrymple, W. F. Loftus, & F. S. Bernardino (Eds.), *Abstracts of the Proceedings of the First Everglades Natural Park Symposium* (pp. 18–19). Hialeah, Florida, USA: Florida National University.
35. Craighead, F. C. Sr. (1969). *The role of the Alligator in shaping plant communities and maintaining wildlife in the Southern Everglades*. Maitland, Florida, USA: Florida Audubon Society.
36. Division SABSS. (2009). Crocodiles in captivity (SANS 631:2009). South African Bureau of Standards.
37. Douglas, R. M. (1990). Volume determination of reptilian and avian eggs with practical applications. *South African Journal of Wildlife Research*, *20*(3), 111–117.
38. Jarque, C. M., & Bera, A. K. (1987). A test for normality of observations and regression residuals. *International Statistical Review /Revue Internationale de Statistique*, *55*(2), 163–172.
39. Wang, T. Y., & Nguang, S. K. (2007). Low cost sensor for volume and surface area computation of axi-symmetric agricultural products. *Journal of Food Engineering*, *79*, 870–877.
40. Blanco, A. E., Icken, W., Ould-Ali, D., Cavero, D., & Schmutz, M. (2014). Genetic parameters of egg quality traits on different pedigree layers with special focus on dynamic stiffness. *Poultry Science*, *93*, 2457–2463.
41. Sarica, M., Onder, H., & Yamak, U. S. (2012). Determining the most effective variables for egg quality traits of five hen genotypes. *International Journal of Agriculture and Biology*, *14*, 235–240.
42. Ferguson, M. W. J. (1982). The structure and composition of the eggshell and embryonic membranes of Alligator mississippiensis. *The Transactions of the Zoological Society of London*, *36*, 99–152.
43. McIlhenney, A. (1935). *The alligator's life history*. Springville, Utah, USA: Christopher Publishing House.
44. Reese, A. M. (1915). *The alligator and its allies*. New York City, New York, USA: G. P. Putnams Sons.
45. Bigalke, R. (1931). Note on the egg of the Nile Crocodile (*Crocodylus niloticus*). *Proceedings of the Zoological Society of London*, *101*, 557–559.

46. Guibe, J. (1970). La reproduction. Traité de Zoologie. In P. Grasse (Ed.), *Glandes endocrines–Embryologie–Systématique–Paléontologie* (14(3) pp. 859–892). Paris: Masson et Cie.
47. Pooley, A. C. (1962). The Nile crocodile, *Crocodilus niloticus*: Notes on the incubation period and growth rate of juveniles. *Larnmergeyer*, *2*, 1–55.
48. Pooley, A. C. (1969). Preliminary studies on the breeding of the Nile crocodile, *Crocodilus niloticus* in Zululand. *Larnmergeyer*, *3*(10), 22–44.

How to cite this article: Lensink, A. V., Swan, G. E., & Myburg, J. G. (2023). The structure of the eggshell and eggshell membranes of *Crocodylus niloticus*. *Journal of Microscopy*, *290,* 23–39. https://doi.org/10.1111/jmi.13173